Preparation of Poly(Acrylonitrile–Butadiene–Styrene)/Montmorillonite Nanocomposites and Degradation Studies During Extrusion Reprocessing

E.-K. Karahaliou, P. A. Tarantili

Laboratory of Polymer Technology, School of Chemical Engineering, National Technical University of Athens, GR 157 80, Zographou, Athens, Greece

Received 18 November 2008; accepted 29 January 2009
DOI 10.1002/app.30158
Published online 27 April 2009 in Wiley InterScience (www.interscience.wiley.com).

ABSTRACT: In this study, the preparation of organically modified montmorillonite/poly(acrylonitrile–butadiene–styrene) (ABS) nanocomposites was studied by melt blending in a twin-screw extruder. The composite material was subjected to a series of five extrusion cycles, and the effect of reprocessing on the material's structural properties was investigated. More specifically, chemical changes were studied with attenuated total reflectance/Fourier transform infrared analysis, the thermal response was recorded by differential scanning calorimetry experiments, and the thermal stability was detected with thermogravimetric analysis. Also, the rheological properties of these blends were investigated via melt flow index tests as a measure of their processability during melt mixing and molding processes. Furthermore, the mechanical strength of the obtained mixtures was explored, and the observed interactions were interpreted in terms of the influence of each component on the functional properties of the final mixture. This attempt enriched our knowledge about the recycling of ABS, with the additional aspect of the use of collected data from more complex systems, that is, composite materials, where the montmorillonite nanoparticles play a role in the interactions initiated by repeated processing. The experimental results of this study show that the reprocessing of ABS/montmorillonite induced oxidation products, but the rheological, mechanical, and thermal properties and the thermal and color stabilities of the composites remained almost stable. J Appl Polym Sci 113: 2271–2281, 2009

Key words: clay; degradation; extrusion; nanocomposites; recycling

INTRODUCTION

Poly(acrylonitrile–butadiene–styrene) (ABS) is a popular engineering thermoplastic because of its unique properties, including an excellent mechanical response, chemical resistance, fine surface appearance, and good processing characteristics. It consists of a styrene–acrylonitrile (SAN) continuous phase partially grafted onto a dispersed polybutadiene phase of an elastomeric nature.

ABS is widely used in the automotive industry, telecommunications, business machines, and consumer market mainly because its property–price profile is intermediate between the lower priced commodity thermoplastics and the more expensive high-performance engineering plastics. For these reasons, ABS is also an interesting material for recycling. ABS polymers are susceptible to oxidative degradation when they are exposed to heat, mechanical stress, and ionizing or ultraviolet radiation in the presence of oxygen because of the formation of reactive intermediates such as free radicals and hydroperoxides. Changes in the chemical structure of polymers as a result of degradation leads to changes in the molecular mass, degree of crystallinity, and mechanical properties.[1]

Because the recycling of industrial plastic scrap would not offer the best performances because of property deterioration after the reprocessing of the polymers, different ways of improving the mechanical properties are necessary, such as stabilization with appropriate additives or reinforcement. A variety of additives, such as light and heat stabilizers and antioxidants, are usually included in ABS formulations to protect its structure and extend the polymer lifetime.[2] In recent years, nanotechnology has opened new avenues in this field. Accordingly, in this article, we focus our attention on the procedure of the incorporation of layered-silicate clays into the recycled polymer matrix as a technique for yielding considerable improvement in the physical and mechanical properties of the recycled material and, ultimately, for increasing the life cycles and versatility of such materials.

The most commonly used clay is sodium montmorillonite (MMT), which is hydrophilic and, therefore, shows restricted compatibility with many polymers.

Correspondence to: P. A. Tarantili (taran@chemeng.ntua.gr).

To obtain good interfacial adhesion for improved mechanical properties, the clay needs to be modified before incorporation into the usual organophilic polymer matrices. Clay modification can be achieved by an ion-exchange reaction with organophilic cations.[3]

Clay possess a net negative charge on its lamellar surface, and therefore, it can absorb cations, such as Na^+ or Ca^{2+}. Alkyl ammonium ions can replace metal cations through the cation-exchange process and occupy the gallery space between nanoscaled layers of the clay to alter the original silicate surface from being hydrophilic to being organophilic.[4] Because of the negative charge of the silicate layer, the cation's head group of an alkyl ammonium molecule preferentially resides at the layer surface with the aliphatic tails being removed from the surface.[5]

Nanocomposites can be prepared by solvent casting, *in situ* polymerization, and melt compounding.[6] So far, the melt intercalation method has been the most commonly used procedure because of its advantages, especially from the commercial point of view and its mass production ability.

Three types of polymer/clay composites are usually recognized: (1) conventional composites, in which the clay is added as a common filler; (2) intercalated nanocomposites, in which a small portion of the polymer is inserted into the interlayer spacing between the layered silicates; and (3) exfoliated nanocomposites (also known as delaminated nanocomposites), in which the silicate layers are almost or completely separated and dispersed in a continuous matrix.

When nanocomposites are prepared by melt mixing, the exfoliation and dispersion of nanoclays in a polymer matrix depend on the organic modifier of the nanoclay, the initial interlayer spacing, the compatibility of the polymer matrix toward the nanoclay, the type and concentration of any added compatibilizer, the viscosity of the resin, and the operational conditions. Although shear is a very important factor, it does not itself provide nanometric dispersion of the clay. The interfacial adhesion needs to be higher to achieve better clay dispersion and, therefore, better performance of the composite.[7]

With regard to melt processing, for polymers that require high melting temperatures (T_m's), the thermal stability of the organic component of the modified clay becomes a significant factor because it limits the top temperature for polymer processing.

ABS/MMT composites have been prepared by melt processing in a twin-screw extruder[8–11] and with a two-roll mill[12,13] or an internal mixer.[14] Masterbatch approaches for improving exfoliation have also been investigated by Wilkie and Zheng[15] and Zhang et al.;[16] also, emulsion and *in situ* polymerization efforts were reported by Jang et al. Pourabas et al.[17] prepared ABS/MMT nanocomposites using a solvent/nonsolvent method.

In this study, we attempted to prepare ABS/MMT nanocomposites by melt processing in a twin-screw extruder. The effects of reprocessing on the prepared nanocomposites were also studied. In addition, the rheological properties via melt flow index (MFI) tests, as a measure of their processability during melt mixing, chemical changes, and thermal and mechanical responses of the obtained materials were recorded. This would be a significant contribution to the recycling of engineering plastics, with the additional aspect of upgrading as-received waste ABS via the incorporation of clay reinforcement.

EXPERIMENTAL

Materials

The easy flowing ABS grade, suitable for injection molding, with the trade name Terluran GP-22 (BASF, Ludwigshafen, Germany), exhibited high resistance to impact and heat deflection.

Commercial organically modified montmorillonite (OMMT) clays under the trade names Cloisite 15A, Cloisite 20A, and Cloisite 30B (Southern Clay Products, Inc., Gonzales, TX) were used. The main characteristics are presented in Table I.

Methods

Blending of the ABS/clay composites

The ABS/OMMT composites were prepared in a corotating twin-screw extruder with a length/diameter ratio of 25 and diameter of 16 mm (Haake PTW 16, Karlsruhe, Germany). The nominal extrusion temperature for ABS was 200°C. It was, therefore, critical to adjust the optimum extrusion temperature for the processing of the polymer mixtures to avoid thermal degradation of the organic modification of MMT because of overexposure of the melt.

The extruder was heated at five zones along the cylinder and the die, according to the temperature profile presented in Table II. Different screw rotation speeds were tested, 35, 100, and 200 rpm, to examine their effects on the clay dispersion in the polymer matrix. Finally, the velocity of the screw was kept at 200 rpm for all of the runs. A circular die with an opening 2 mm in diameter was mounted to the extruder.

As a simulation of the recycling process, the ABS composite was subjected to five repeated cycles of extrusion.

After melt mixing, the obtained material in the form of a continuous strand was granulated with a Brabender (Duisburg, Germany) pelletizer.

TABLE I
Main Characteristics of the Nanoclays

	Cloisite 15A	Cloisite 20A	Cloisite 30B
Organic modifier	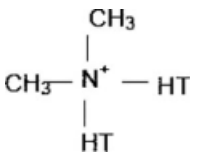	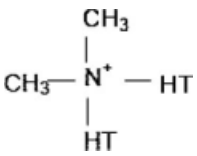	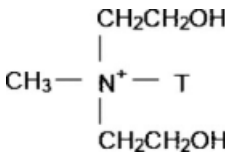
	Dimethyl, dihydrogenated tallow, quaternary amonium	Dimethyl, dihydrogenated tallow, quaternary amonium	Methyl, tallow, bis-2-hydroxylethyl, quaternary ammounium
Modifier concentration	125 mequiv/100 g of clay	95 mequiv/100 g of clay	90 mequiv/100 g of clay
Weight loss in ignition (%)	43	38	30

HT = hydrogenated tallow (~ 65% for C18, ~ 30% for C16, and ~ 5% for C14); T = tallow (~ 65% for C18, ~ 30% for C16, and ~ 5% for C14).

Injection molding

Injection molding was performed with an Arburg (Lossburg, Germany) 221K Allrounder machine equipped with a screw 25 mm in diameter and a clapping unit force of 350 kN. The processing parameters for the preparation of the 1% (w/w) Cloisite 30B/ABS composites are presented in Table III. The mold was a two-cavity system capable of producing dumbbell specimens for subsequent measurement of the tensile properties (ASTM D 638, specimen type IV).

X-ray diffraction (XRD)

XRD of the clay and nanocomposites, to evaluate the evolution of the clay d_{001} reflection, was performed in a Siemens (Madison, WI) 5000 instrument (35 kV, 25 mA) with Cu Kα X-ray radiation with a wavelength of $\lambda = 0.154$ nm. The diffractograms were scanned in the 2θ range from 2 to 10° at a rate of 2°/min. Samples for X-ray analysis were obtained from compression-molded plaques to avoid any preferred orientation of the clay.

Attenuated total reflectance/Fourier transform infrared (ATR–FTIR) spectroscopy

For the determination of changes in the chemical structure of the ABS specimens after each extrusion cycle, spectroscopic measurements were performed with a Nicolet (Madison, WI) FTIR spectrometer (model Magna IR 750, deuterated triglycine sulfate (DTGS) detector; Nichrome source, beam splitter, KBr). A total of 100 scans were applied with a resolution up to 4 cm^{-1}. Spectra were obtained in the ATR mode with a standard ZnSe 45° flat plate contact sampler (12 reflections; Spectra-Tech, Stanford, CT) on which samples of ABS were placed (100 μL). Spectroscopic data were treated with the standard software (OMNIC 3.1, Nicolet).

All spectra were smoothed with the automatic smooth function of the previously mentioned software, which used the Savitsky–Golay algorithm (five-point moving second-degree polynomial). After this procedure, the baseline was corrected with the automatic baseline correct function.

Color test

Color change (ΔE) values were examined with a microcolor tristimulus colorimeter (Micromatch Plus, Sheen Instruments, Surrey, UK). This instrument was designed to determine color characteristics in the CIELAB color system according to ASTM D 2244-68. The system was an approximately uniform color space using three parameters to define color: the luminance factor (L), which measures the light–

TABLE II
Processing Conditions for the Extrusion of the ABS Composites

	Temperature in extruder zone (°C)						Screw rotation		Feeder screw rotation	
Material (w/w)	1st	2nd	3rd	4th	5th	Die	speed (rpm)	Feeder	speed (rpm)	Vacuum
2% Cloisite 15A/ABS	210	200	200	195	195	190	200	Yes	80	Yes
2% Cloisite 20A/ABS	210	200	200	195	195	190	200	Yes	80	Yes
1% Cloisite 30B/ABS	210	200	200	195	195	190	200/100/35	Yes	80/40/15	Yes
2% Cloisite 30B/ABS	210	200	200	195	195	190	200/100/35	Yes	80/40/15	Yes

TABLE III
Injection-Molding Parameters for the 1% (w/w) Cloisite 30B/ABS Composites

Temperature in screw zone (°C)					Injection pressure (bar)			
1st	2nd	3rd	4th	5th	8 ccm	10 ccm	Packing pressure (bar)	Cooling time (s)
245	235	225	220	125	1000	1150	500	0.5

dark character; the red saturation index (a), which measures the red–green character; and the yellow saturation index (b), which measures the yellow–blue character. ΔE can be calculated with the following equation:

$$\Delta E = \sqrt{(\Delta L)^2 + (\Delta a)^2 + (\Delta b)^2} \quad (1)$$

where ΔL is the change in the luminance index, Δa is the change in a and Δb is the change in b.

Thermogravimetric analysis (TGA)

Thermogravimetric tests in ABS composites were performed with a Mettler Toledo (Schwerzenbach, Switzerland) thermogravimetric analyzer (model TGA-SDTA 851E). The analysis was run with 10-mg samples at a heating rate of 10°C/min from 25 to 700°C in a nitrogen atmosphere.

Differential scanning calorimetry (DSC)

DSC measurements were run in a PerkinElmer (Waltham, MA) model Pyris 6 differential scanning calorimeter with pure indium as a calibration standard. Samples of approximately 10 mg were accurately weighed in an analytical balance and encapsulated in aluminum pans. All runs were conducted under a nitrogen flow of 20 cm^3/min to limit thermooxidative degradation. The samples were heated from 30 to 260°C at a rate of 10°C/min; they remained at this temperature for 5 min to erase the previous thermal history. After this treatment, the samples were cooled from 260 to 30°C at −10°C/min and again heated from 30 to 260°C at the same rate. The glass-transition temperature (T_g), T_m, and heat of fusion were calculated from the thermographs obtained during the second heating cycle.

MFI

The MFI measurements were carried out according to procedure A of the ASTM D 1238 specification in a Kayeness Inc. (Morgantown, PA) model 4004 capillary rheometer. To ensure complete melting, a large enough quantity of each one of the polymer blends (ca. 5 g) was placed in the barrel, where it remained for 180 s before the test was started.

Mechanical tests

Tensile testing was carried out according to ASTM D 638. Five specimens from each composition (with dimensions according to the type IV specimen of the previous specification) were tested with an Instron (model 4466) (Bucks, UK) tensiometer equipped with a load cell with a maximum capacity of 10 kN and operating at a grip separation speed of 50 mm/min.

RESULTS AND DISCUSSION

XRD

XRD technique was used to assess the level of clay dispersion within the polymer matrix. With Bragg's rule ($2d \sin \theta = n\lambda$, where d is the spacing between the planes in the atomic lattice, θ is the angle between the incident ray and the scattering planes, n is an integer determined by the order given, and λ is the wavelength), the basal spacing for the clay layers was obtained.

The XRD patterns for Cloisite 15A and the composite of ABS with 2% Cloisite 15A, prepared through the melt intercalation process are shown in Figure 1. The original basal reflection peak of Cloisite 15A appeared at 2.8°, which corresponded to an intergallery spacing of 3.15 nm, whereas the reflection peak of the 2% (w/w) Cloisite 15A/ABS composite slightly shifted to a lower angle of 2.61°, which corresponded to an intergallery spacing of 3.38 nm (Table IV).

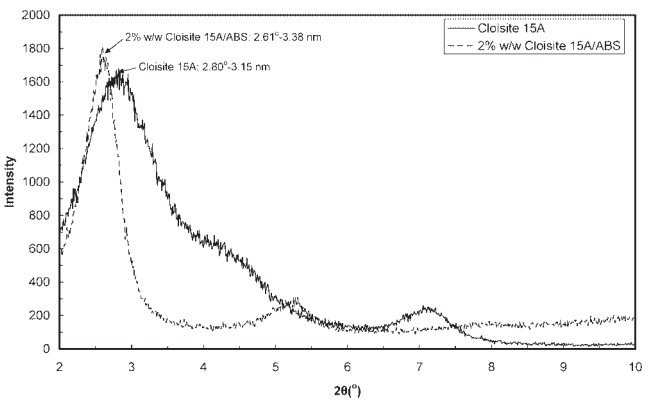

Figure 1 XRD patterns of Cloisite 15A and the 2% (w/w) Cloisite 20A/ABS nanocomposite.

TABLE IV
Interlayer Spacing of the Clays and OMMT/ABS Composites

OMMT/ABS (w/w; screw rotation speed)	2θ (°)/d_{001} (nm)		
	Cloisite 15A	Cloisite 20A	Cloisite 30B
0	2.80/3.154	3.52/2.505	4.90/1.803
1% (35 rpm)	—	—	2.55/3.465
1% (100 rpm)	—	—	2.48/3.554
1% (200 rpm)	—	—	2.58/3.422
2% (35 rpm)	—	—	2.65/3.334
2% (100 rpm)	2.61/3.378	2.63/3.359	2.62/3.370
2% (200 rpm)	—	—	2.55/3.462

The XRD patterns for Cloisite 20A and the 2% (w/w) Cloisite 20A/ABS composite are shown in Figure 2. The original basal reflection peak of Cloisite 20A appeared at 3.52°, which corresponded to an intergallery spacing of 2.5 nm, whereas the reflection peak of the examined composite shifted to a lower angle of 2.83°, which gave an intergallery spacing of 3.36 nm.

Vaia et al.[19] proposed that an increase in the intergallery spacing, which is related to the intercalation of the polymer through the clay galleries, results in a new diffraction pattern that corresponds to the increased spacing of the clay galleries. According to these authors, the degree of intercalation in the hybrid composite could be determined by changes in the sharpness and intensity of the corresponding reflection peaks.

The Cloisite 30B pattern, shown in Figure 3, showed an intense peak around 2θ = 4.89°, which denoted that the basal spacing in the silicate layers was 1.8 nm. The sample with 2% (w/w) clay showed a well-defined peak at 2.61° with a decreased intensity and intergallery spacing of 3.38 nm. The sample with 1% (w/w) Cloisite 30B showed a significant decrease in the intensity of the diffraction peak, with an intergallery spacing of 3.55 nm. This indicated the possibility of obtaining exfoliated

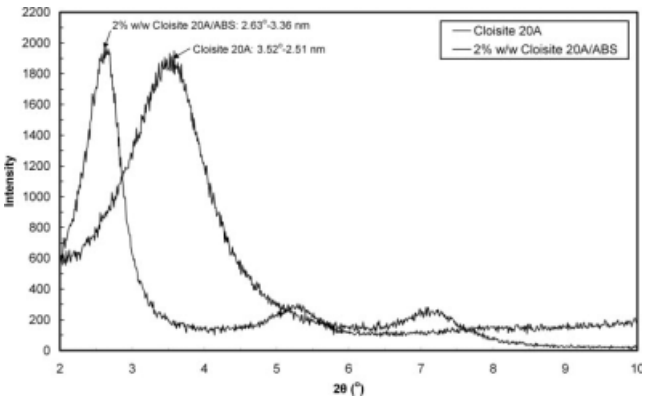

Figure 2 XRD patterns of Cloisite 20A and the 2% (w/w) Cloisite 20A/ABS nanocomposite.

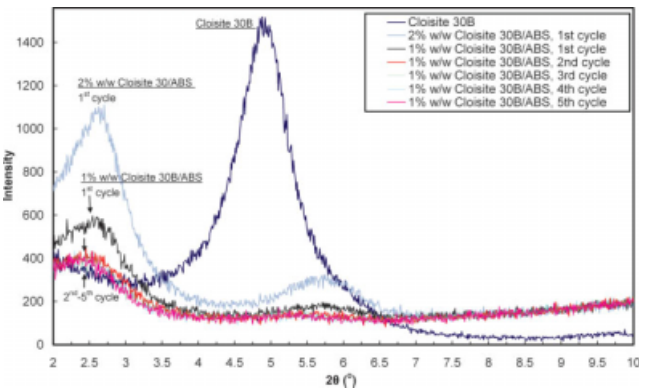

Figure 3 XRD patterns of Cloisite 30B and its composites with ABS after extrusion reprocessing at 100 rpm. [Color figure can be viewed in the online issue, which is available at www.interscience.wiley.com.]

or intercalated silicate nanolayers of clay dispersed in the ABS matrix.

As shown in Table IV, the screw rotation speed did not have any significant effect on the dispersion of clay in the ABS matrix. However, reprocessing in the twin screw extruder improved the dispersion and intercalation of clay in the polymer matrix after the second cycle, as is obvious in Figure 3.

MFI

The incorporation of 1% (w/w) nanoclays in ABS decreased the flow rate of the mixture compared with that of pure ABS, which was a result of the increase in the system viscosity (Table V). Similar results were reported by Aalaie and Rahmatpour,[14] who studied the rheological behavior of ABS nanocomposites at low shear rates. The confinement of polymer chain motion caused by organoclay platelets and tactoids in the ABS matrix, together with interactions between the polar groups of ABS and oxygen groups of Cloisite 30B, may have caused this effect. However, at high shear rates, the flow properties of the composite were comparable to those of pure ABS. This behavior was attributed to the preferential orientation of clay layers, or even anisotropic tactoids, parallel to the flow direction.

TABLE V
MFI Measurements of the 1% (w/w) OMMT/ABS Composites as a Function of Extrusion Processing

Number of reprocessing cycles	MFI (g/10 min)
1	1.161 ± 0.165 (1.507 ± 0.181)[a]
2	1.181 ± 0.173
3	1.199 ± 0.120
4	1.204 ± 0.144
5	1.247 ± 0.136

[a] Pure ABS.

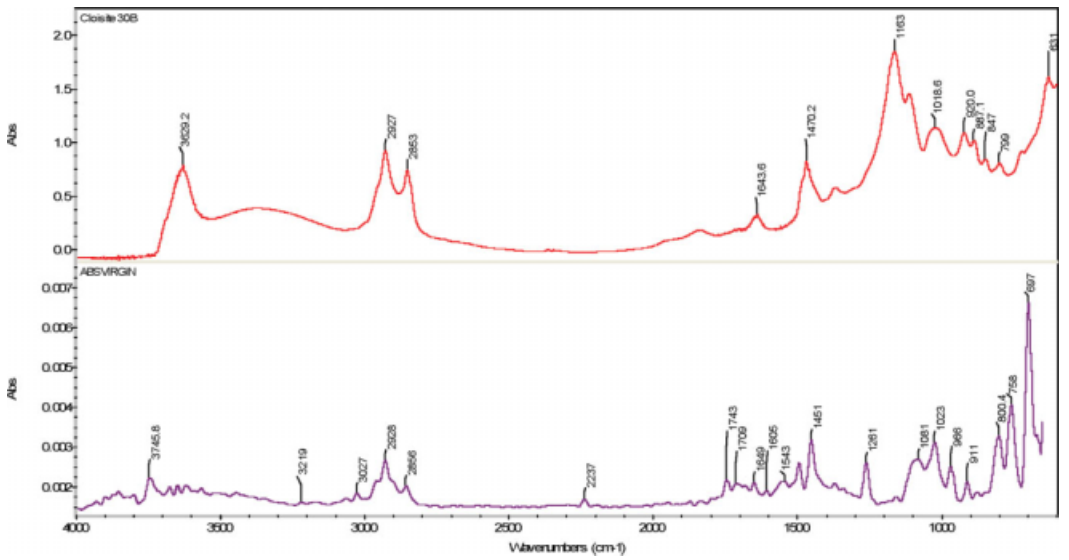

Figure 4 ATR–FTIR spectra of Cloisite 30B and virgin ABS. [Color figure can be viewed in the online issue, which is available at www.interscience.wiley.com.]

From the first to fifth extrusion cycle, a slight increase in the MFI values was observed, which was, however, in the range of statistical error. In agreement with our results, Boldizar and Möller[20] reported almost constant values of melt volume flow rate (MVR) after repeated extrusion of ABS. However, in the experimental setup containing a combination of extrusion and accelerated aging, after the fourth cycle, there was a significant increase in the MVR values because of the consumption of antioxidant stabilizers during extrusion. It is, therefore, reasonable that the elimination of the previous additives resulted in a less protected ABS during the following thermooxidative aging process. The oxidation of the grafted polybutadiene can lead to a degrafting of SAN, which was in agreement with the observed increase in MVR.

ATR–FTIR

The representative ATR spectra of Cloisite 30B, ABS, and the 1% (w/w) Cloisite 30B/ABS composites after each extrusion cycle are presented in Figures 4 and 5. Cloisite 30B showed absorption bands at 3630 and 3367 cm^{-1}, which derived from O—H stretching for the silicate group and water, respectively; 1643 cm^{-1} (related to O—H bending); 1018 cm^{-1} (stretching vibration of Si—O—Si from silicate); and 920

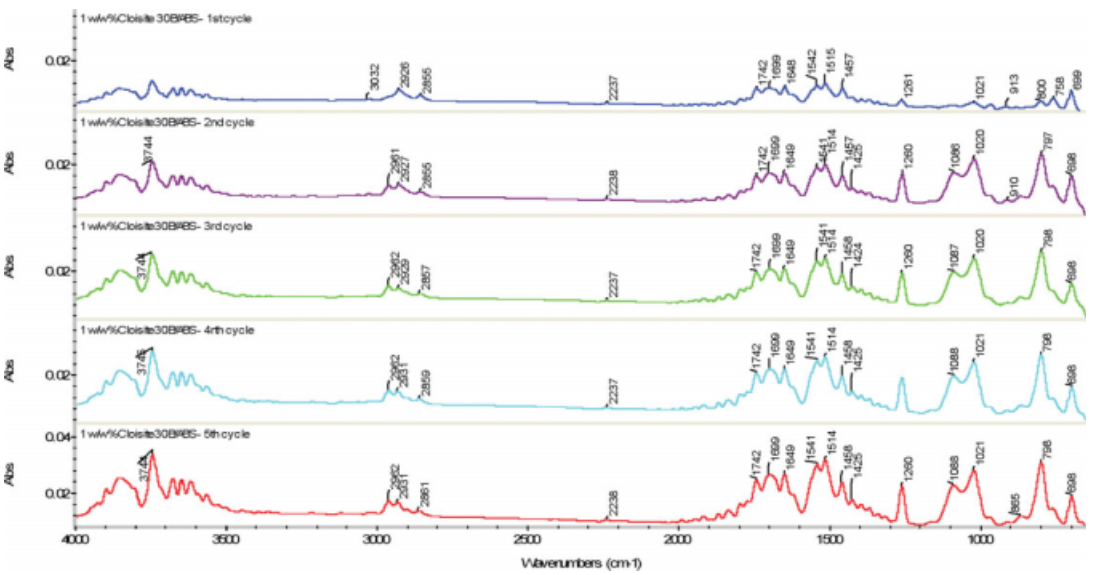

Figure 5 ATR–FTIR spectra of the 1% (w/w) OMMT/ABS composite as a function of extrusion processing. [Color figure can be viewed in the online issue, which is available at www.interscience.wiley.com.]

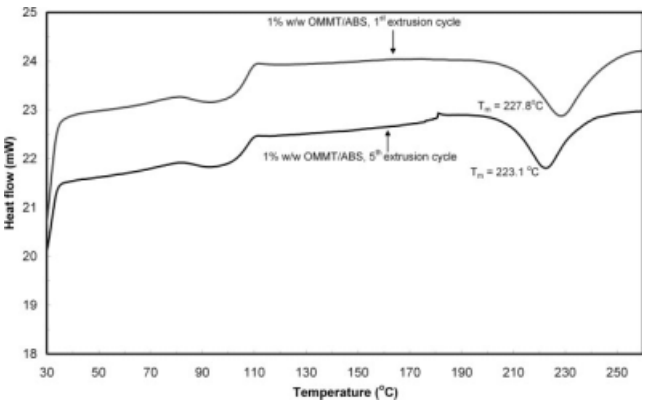

Figure 6 DSC curves of the 1% (w/w) OMMT/ABS composite (first heating cycle).

cm^{-1} (Al—OH—Al deformation of aluminates).[21] The organic modification was responsible for the bands located at 2927, 2853, and 1470 cm^{-1}, which were assigned to C—H vibrations of methylene groups (asymmetric stretching, symmetric stretching, and bending, respectively).

The spectra of the 1% Cloisite 30B/ABS composites are presented in Figure 5. The aromatic and aliphatic C—H stretching was clearly be seen in the range 3200–3000 and 3000–2800 cm^{-1}, respectively. The intense and well-defined C≡N stretching from acrylonitrile was seen at 2237 cm^{-1}. The scissoring mode of CH_2 groups was at 1457 cm^{-1}, and the intense ring bends were visible at 798 and 698 cm^{-1}.

Typical dienic rubber bands were easy to identify in the range 1000–900 cm^{-1} as follows: the absorption peak at 998 cm^{-1} corresponded to off-frequency vibrations of CH in CH=CH groups, the band at 967 cm^{-1} was due to off-frequency vibrations of CH in *trans*-CH=CH— moieties, and the band at 913 cm^{-1} was determined by off-frequency vibrations for $=CH_2$. The deformation vibration for $=CH_2$, which usually appears at wavelengths under 1465 cm^{-1}, shifted to 1457 cm^{-1} because of the influence of the double bond. The bands in the interval 2950–2800 cm^{-1} were attributed to asymmetric and symmetric $—CH_2$ groups.

Thermomechanical degradation due to the repeating extrusion processing of ABS produced oxygen-containing groups such as esters, hydroxyls, carboxyls, and carbonyls. Chemical processes can be followed by the emergence of new peaks in the area of hydroxyl (3600–3200 cm^{-1}), carbonyl (1850–1600 cm^{-1}), and ester groups (1300–1000 cm^{-1}) and by changes in the reference signals for the styrene, acrylonitrile, and butadiene components in ABS.

To quantify the aforementioned chemical changes introduced by extrusion reprocessing of the OMMT/ABS composites, the carbonyl index was determined as the ratio of integrated band absorbance of carbonyls around 1850–1600 cm^{-1} to the absorbance of $—CH_2$ bands at 2950–2800 cm^{-1}. The ester groups (C—O stretching) were quantified by the integration of the band absorbance of 1261 cm^{-1} and the bands around 1100–1000 cm^{-1}. The butadiene and acrylonitrile changes were recorded through the integration of the 913- and 2237-cm^{-1} peaks, respectively. The results of the previous analysis are presented in Table VI.

The hydroxyl peak appeared as a broad signal with a maximum at about 3650 cm^{-1}, typical of an OH stretch. The area of this peak became significant after the second extrusion process and gradually increased after each extrusion cycle. This peak suggested the formation of oxidized species and, further, some kind of thermooxidation taking place in the polymer.

Similar behavior was observed for the carbonyl absorption (1850–1600 cm^{-1}) and ester bands (1261- and 1100–1000 cm^{-1} bands). On the basis of the results shown in Table VI, we concluded that the carbonyl group concentration increased gradually during the extrusion processing but to a lower extent compared with that of the ester groups. On the other hand, the ester groups showed a dramatic increase from the first to the second extrusion processing, which then became lower up to the fifth extrusion pass.

The lower intensity of the peaks around 1000–950 cm^{-1} indicated that the butadiene phase decreased and some degradation should have been expected, which was attributed to chain scission and crosslinking. This behavior was depicted in the values of the area of the 913 cm^{-1} peak versus extrusion cycle shown in Table VI.

The band corresponding to the —C≡N group, present in acrylonitrile, remained almost intact, and

TABLE VI
Normalized Integrated Area of ATR Bands for the OMMT/ABS Composites as a Function of Extrusion Processing

Number of reprocessing cycles	2237 cm^{-1}	1850–1600 cm^{-1}	1261 cm^{-1}	1100–1000 cm^{-1}	913 cm^{-1}
1	0.033	3.02	0.178	0.521	0.062
2	0.038	3.78	0.702	3.751	0.042
3	0.034	5.09	0.878	4.711	0.027
4	0.036	5.33	0.832	4.234	0.035
5	0.033	5.83	0.878	4.426	0.040

TABLE VII
Change in the Luminance Index (Δ*L*), Change in the Red Saturation Index (Δ*a*), and Change in the Yellow Saturation Index (Δ*b*) After the Reprocessing of the 1% (w/w) OMMT/ABS Composites

Number of reprocessing cycles	Δ*L*	Δ*a*	Δ*b*	Δ*E*
1	−5.91 ± 1.94	3.62 ± 0.66	13.176 ± 2.20	14.92 ± 2.79
2	−4.49 ± 3.01	3.23 ± 0.34	11.27 ± 0.89	12.86 ± 1.12
3	−6.72 ± 0.76	3.76 ± 0.26	11.81 ± 1.32	14.12 ± 1.23
4	−9.28 ± 0.82	4.11 ± 0.57	11.90 ± 1.35	15.70 ± 0.93
5	−9.72 ± 0.67	4.63 ± 0.28	12.58 ± 0.77	16.56 ± 0.91

therefore, this group seemed to be relatively stable under these processing conditions.

ABS is sensitive to oxidation because of the presence of polybutadiene units, which act as oxidation sensitizers and lead to the formation of carbonyl groups, which absorb at 1670–1750 cm^{-1}.[22] The study of the effect of repeated injection molding in the properties of polycarbonate/ABS blends by Eguiazábal and Nazábal[23] revealed a new peak in ABS at 1680 cm^{-1}, which was not present in unprocessed ABS. They also observed that the intensity of this peak increased with the number of processing cycles, and this was attributed to the appearance of a ketonic group. On the other hand, Bai et al.[23] did not observe any absorption due to carbonyl groups even after reprocessing at high temperatures (270°C).

Color test

The Δ*E* values in terms of the CIELAB scale are presented in Table VII. The ABS composites presented very stable behavior during the repeated extrusion cycles, and only *L* shifted to lower values. The *a*, *b*, and total Δ*E* values remained almost stable.

DSC

Typical DSC curves of the ABS resin after the first and fifth extrusion cycle are presented in Figures 6 and 7. The T_g values of ABS as derived from the DSC runs are listed in Table VIII. The glass transition of the SAN phase was determined to be at approximately 103°C. The DSC thermographs revealed a fairly constant T_g of 103 ± 1°C for the ABS nanocomposites from the extrusion series, which was expected for the SAN phase of ABS. Similar behavior was reported during repeated extrusion processing in ABS samples. However, during accelerated aging, a gradual increase in the T_g values was recorded with increasing number of cycles, possibly because of physical aging.[20]

An increase in the glass transition of the rubber phase (butadiene) was reported by Blom et al.[25] in their study of ABS degradation via DSC. This was explained by the fact that this phase is most susceptible to oxidative degradation, which leads to crosslink formation and decreased chain mobility. According to this study, this degradation was responsible for the mechanical property reduction and only proceeded at an appreciable rate at elevated temperatures in the presence of oxygen. Increases in the T_g values of the rubber phase after reprocessing due to crosslinking reactions were reported by Eguiazábal and Nazábal[23] and Bai et al.[24] with dynamic mechanical analysis.

T_m remained stable between the first and third extrusion cycle, but a decrease of about 4°C was found for the last two extrusion cycles. No significant effect on the melting enthalpy during the repeated processing of ABS was observed.

TGA

The decomposition temperature of Cloisite 30B was above 300°C, and this was attributed to the decomposition of the organic modifier. This suggests that, during melt reprocessing, which was carried out around 200°C, the organic modifier in the clay remained active and facilitated dispersion and, further, the attempt to achieve an exfoliated or intercalated structure, as it was confirmed to some extent by the XRD patterns. As is obvious from Table IX and Figure 8, extrusion processing did not have any

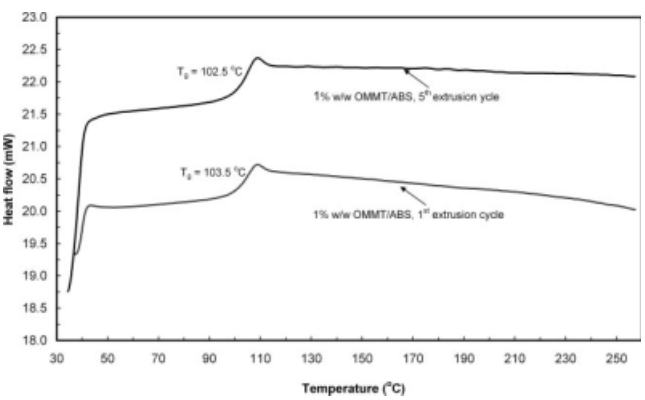

Figure 7 DSC curves of the 1% (w/w) OMMT/ABS composite (second heating cycle).

TABLE VIII
DSC Analysis Data for the 1% (w/w) OMMT/ABS Composites as a Function of Extrusion Processing

Number of reprocessing cycles	First heating cycle		Second heating cycle
	T_m (°C)	Melting enthalpy peak (J/g)	T_g (°C)
1	227.78 ± 1.04 (224.59)[a]	14.06 ± 3.87 (9.62)	103.50 ± 1.78 (102.38)
2	227.14 ± 1.93	17.28 ± 0.81	103.04 ± 0.36
3	226.63 ± 0.71	14.95 ± 0.58	102.07 ± 0.56
4	224.73 ± 1.29	14.29 ± 1.61	102.44 ± 0.02
5	223.10 ± 0.87	14.83 ± 2.5	102.48 ± 0.46

[a] Virgin ABS.

significant effect on the temperature of the maximum thermal degradation rate, whereas a slight decrease in the onset temperature of thermal degradation was observed as a result of the repeated extrusion cycles. Finally, the char residue increased to about 0.7%, which was obviously a result of the incorporation of the inorganic clay, which remained as a residue and contributed to the final weight. The TGA studies of Yeh et al.[13] made with ABS nanocomposites in air showed an enhancement in the thermal stability and an increase in the remaining residue.

Similarly, Patiño-Soto et al.[11] observed that dispersed clay enhanced the thermal stability of ABS because the intercalated or exfoliated clays displayed barrier properties against the diffusion of atmospheric oxygen into the material, which inhibited oxidative attack of the system. Similar results were reported by Kim et al.,[10] and the observed effect was attributed to the shielding effect of the clay layers. According to Zanetti et al.,[26] the layers of organomodified silicate act as a barrier to small molecules generated during the thermal degradation process, and therefore, degradation products have to take the long way around the clay layers. Therefore, the addition of organoclay to a polymer matrix is expected to slow down the release rate of decomposed products to endow the degradation products more chances to bind back to the undecomposed original polymer matrix. Moreover, because TGA is a dynamic experiment, another possible reason for the increase in the decomposition temperature of the ABS nanocomposites was the increase in viscosity due to the addition of clay, which would have inhibited transmission; that is, it would have increased the difficulty for the inward diffusion of oxygen and the outward diffusion of the degradation byproducts.

The ABS samples with higher acrylonitrile contents produced a greater increase in the decomposition temperature, which was attributed to better clay intercalation/exfoliation due to the higher polarity brought about by the higher acrylonitrile content.

On the basis of the previous discussion of the related literature, we drew the conclusion that our nanocomposites did not display an improvement in their thermal stability as a result of their structure. In fact, the data obtained from XRD analysis revealed that we did not succeed in producing fully exfoliated structures, which probably would have led to an essential improvement in the thermal resistance and prevention of thermal degradation during the TGA experiments.

TABLE IX
TGA Data for the 1% (w/w) OMMT/ABS Composites

Number of reprocessing cycles	Onset temperature of thermal degradation (°C)	Temperature of the maximum thermal degradation rate (°C)	Char residue (%)
1	403.03 (407.29)[a]	427.33 (428.33)	3.57 (2.89)
5	402.16	427.00	3.75

[a] Virgin ABS.

Tensile testing

As shown in Table X, the incorporation of Cloisite 30B in ABS did not have any significant effect on the

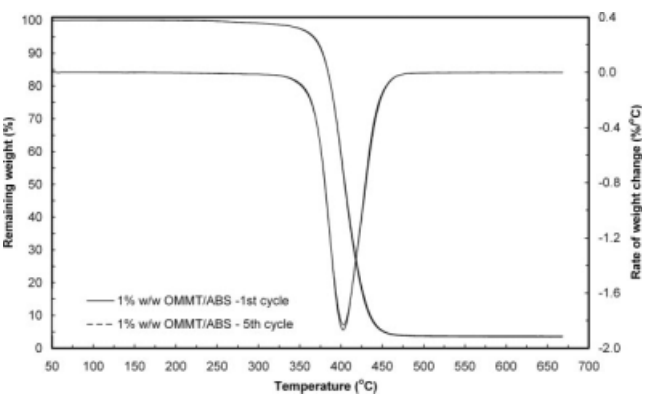

Figure 8 TGA curves of the 1% (w/w) OMMT/ABS composite after the first and fifth extrusion cycles.

TABLE X
Tensile Test Results for the 1% (w/w) OMMT/ABS Composites During Extrusion Reprocessing

Number of reprocessing cycles	Tensile strength (MPa)	Modulus of elasticity (MPa)	Strain at break (%)
1	50.79 ± 0.62 (50.33 ± 1.79)	2117.91 ± 159.05 (1939.75 ± 103.84)	6.69 ± 2.58 (11.25 ± 3.2)
2	51.26 ± 1.64	2040.26 ± 115.23	7.28 ± 0.84
3	51.28 ± 0.79	2160.01 ± 94.31	5.98 ± 1.33
4	51.22 ± 0.63	2065.14 ± 47.64	6.75 ± 2.85
5	50.63 ± 0.66	2170.34 ± 101.54	5.65 ± 1.14

tensile strength, but it increased the tensile modulus and decreased the elongation at break of the reinforced samples in comparison with pure ABS.

Aalaie and Rahmatroup[14] reported decreases in the tensile strength and elongation of ABS/Cloisite 30B nanocomposites in comparison with those of pure ABS. Su et al.[27] reported a decrease in the tensile properties of ABS/clay hybrids despite the intercalated/exfoliated structure formation. However, Zhang et al.[28] believed that the formation of an exfoliated nanocomposite did not improve the mechanical properties of ABS. In addition, a plasticization effect of organically modified clay may reduce the mechanical properties of nanocomposites.[29]

Using different types of surfactant-modified clays for ABS reinforcement, Stretz et al.[9] observed that the elongation at break decreased and the yield strength remained about the same. However, for some clays, an increased MMT content resulted in a slight increase in the yield strength. Yeh et al.[13] found that the incorporation of organoclay platelets into a polymer matrix increased the tensile strength of ABS for concentrations up to 3 wt %. Higher amounts of organoclay loading (5 wt %) were found to decrease the tensile strength of the nanocomposite material. On the other hand, the elongation at break decreased as the organoclay loading increased in the composite.

Kim et al.[10] reported increases in the tensile strength and elongation at break of ABS composites reinforced with unmodified Cloisite 25A and modified with tetrasulfane.

As shown in Table X, reprocessing in a twin-screw extrusion did not affect the tensile properties of the ABS nanocomposites. Similar results were reported by Boldizar and Möller[20] with regard to the elongation at break after the reprocessing of pure ABS in a single-screw extruder. However, during the test accompanied by accelerating aging, the elongation exhibited a marked oscillating behavior after the first cycle.

A recycling simulation of ABS was performed by Bai et al.,[24] who used an appropriate combination of a granulator, torque rheometer, and injection-molding machine. The modulus of elasticity did not change significantly with increasing number of reprocessing cycles, but the tensile strength increased slightly. This small increase in the strength was related to the loss of small molecules and crosslinks in the rubber phase. The processing temperature and rotational speed of rheometer had a minor effect on the tensile properties of ABS.

CONCLUSIONS

The mechanical recycling of ABS through melt processing in a twin-screw extruder was a simple method that did not affect the processing characteristics of the material up to five repeated extrusion cycles.

Intercalated or/and partially exfoliated composite structures of OMMT/ABS were prepared by melt mixing in a twin-screw extruder. Screw rotation speed did not have a significant effect on the composite structure; however, the second extrusion cycle improved the dispersion efficiency of the system.

The reprocessing of the OMMT/ABS composites in a twin-screw extruder increased the oxidation products progressively between the repeated cycles, as was recorded with ATR/FTIR analysis. The color of the samples was rather stable between successive extrusion cycles. T_m decreased slightly, and T_g was almost stable. The thermal degradation of the material was not affected by repeated extrusion, as was observed by TGA. Finally, the rheological and tensile properties of the composites did not present any significant change with increasing number of reprocessing cycles.

On the basis of the previous discussion, the OMMT nanoparticles not only acted as reinforcement for ABS but also seemed to play a role in the interaction taking place during the aging of ABS repeated through melt processing.

References

1. Bokria, J. G.; Schlick, S. Polymer 2002, 43, 3239.
2. Scott, G. In Macromolecular and Polymer-Bound Antioxidants; Scott, G., Ed.; Elsevier: Amsterdam, 1993; Vol. II, Chapter 5.
3. Utracki, L. A. Clay-Containing Polymeric Nanocomposites; Rapra Technology: Shropshire, England, 2004; Vol. 1, Chapter 2.
4. Burnside, S. D.; Giannelis, E. P. Chem Mater 1995, 7, 1597.

5. Chen, G. X.; Yoon, J. S. Polym Int 2005, 54, 939.
6. Pinnavaia, T. J.; Beall, G. W. Polymer Clay Nanocomposites; Wiley: Chichester, England, 2002; Chapter 5.
7. Patiño-Soto, A. P.; Sánchez-Valdes, S.; Ramos-Devalle, L. F. J Polym Sci Part B: Polym Phys 2008, 46, 190.
8. Wang, S.; Hu, Y.; Song, L.; Liu, J.; Chen, Z.; Fan, W. J Appl Polym Sci 2004, 91, 1457.
9. Stretz, H. A.; Paul, D. R.; Cassidy, P. E. Polymer 2005, 46, 3818.
10. Kim, H.-S.; Park, B. H.; Choi, J. H.; Yoon, J.-S. J Appl Polym Sci 2008, 107, 2539.
11. Patiño-Soto, A. P.; Sánchez-Valdes, S.; Ramos-Devalle, L. F. Macromol Mater Eng 2007, 292, 302.
12. Xiao, J.; Hu, Y.; Lu, H.; Cai, Y.; Chen, Z.; Fan, W. J Appl Polym Sci 2007, 104, 2130.
13. Yeh, J.-M.; Chen, C.-L.; Huang, C. C.; Chang, F.-C.; Chen, S.-C.; Su, P.-L.; Kuo, C.-C.; Hsu, J.-T.; Chen, B.; Yu, Y.-H. J Appl Polym Sci 2005, 99, 1576.
14. Aalaie, J.; Rahmatpour, A. J Macromol Sci Phys 2007, 46, 1255.
15. Wilkie, C. A.; Zheng, X. Polym Degrad Stab 2003, 82, 441.
16. Zhang, B.; Song, M.; Hao, G.; Guo, T. J Appl Polym Sci 2004, 94, 238.
17. Jang, L. W.; Kang, C. M.; Lee, D. C. J Polym Sci: Part B: Polym Phys 2001, 39, 719.
18. Pourabas, B.; Raeesi, V. Polymer 2005, 46, 5533.
19. Vaia, R. A.; Ishii, H.; Giannelis, E. P. Chem Mater 1993, 5, 1694.
20. Boldizar, A.; Möller, K. Polym Degrad Stab 2003, 81, 359.
21. Bora, M.; Ganguli, J. N.; Dutta, D. K. Thermochim Acta 2000, 346, 169.
22. Dong, D.; Tasaka, S.; Aikawa, S.; Kamiya, S.; Inagaki, N.; Inoue, Y. Polym Degrad Stab 2001, 73, 319.
23. Eguiazábal, J. I.; Nazábal, J. Polym Eng Sci 1990, 30, 527.
24. Bai, X.; Isaak, D. H.; Smith, K. Polym Eng Sci 2007,120.
25. Blom, H.; Yeh, R.; Wojnarowski, R.; Ling, M. Thermochim Acta 2006, 442, 64.
26. Zanetti, M.; Camino, G.; Mulhaupt, R. Polym Degrad Stab 2001, 74, 413.
27. Su., S.; Jiang, D. D.; Wilkie, C. A. Polym Degrad Stab 2004, 83, 333.
28. Zhang, J.; Jiang, D. D.; Wilkie, C. A. Polym Degrad Stab 2006, 91, 358.
29. Zhang, J.; Jiang, D. D.; Wang, D.; Wilkie, C. A. Polym Degrad Stab 2006, 91, 2665.